Applied Physics Letters

A quantum-based power standard: Using Rydberg atoms for a SI-traceable radio-frequency power measurement technique in rectangular waveguides

Cite as: Appl. Phys. Lett. **113**, 094101 (2018); https://doi.org/10.1063/1.5045212
Submitted: 18 June 2018 • Accepted: 14 August 2018 • Published Online: 28 August 2018

Christopher L. Holloway, Matthew T. Simons, Marcus D. Kautz, et al.

APPLIED PHYSICS LETTERS **113**, 094101 (2018)

A quantum-based power standard: Using Rydberg atoms for a SI-traceable radio-frequency power measurement technique in rectangular waveguides

Christopher L. Holloway,[1,a)] Matthew T. Simons,[1] Marcus D. Kautz,[1] Abdulaziz H. Haddab,[1] Joshua A. Gordon,[1] and Thomas P. Crowley[2]
[1]*National Institute of Standards and Technology, Boulder, Colorado 80305, USA*
[2]*Xantho Technologies, LLC, Madison, Wisconsin 53705, USA*

(Received 18 June 2018; accepted 14 August 2018; published online 28 August 2018)

In this work, we demonstrate an approach for determining radio-frequency (RF) power using electromagnetically induced transparency (EIT) in a Rydberg atomic vapor. This is accomplished by placing alkali atomic vapor in a rectangular waveguide and measuring the electric (E) field strength (utilizing EIT and Autler-Townes splitting) for a wave propagating down the waveguide. The RF power carried by the wave is then related to this measured E-field, which leads to a direct International System of Units measurement of RF power. To demonstrate this approach, we first measure the field distribution of the fundamental mode in the waveguide and then determine the power carried by the wave at both 19.629 GHz and 26.526 GHz from the measured E-field. We show comparisons between the RF power obtained with this technique and those obtained with a conventional power meter. https://doi.org/10.1063/1.5045212

The world of measurement science is changing rapidly due to the International System of Units (SI) redefinition planned for late 2018.[1,2] As a result of the shift towards fundamental physical constants, the role of primary standards must change. This includes radio-frequency (RF) power. The current method of power traceability is typically based on an indirect path through a thermal measurement using a calorimeter, in which temperature rise created by absorbed microwave energy is compared to the DC electrical power. A direct SI-traceable measurement of RF power is desired and to accomplish this we will utilize recent work on electric (E) field metrology using Rydberg atomic vapor.

It can be shown that the E-field of the fundamental mode [the transverse electric (TE_{10}) mode] in the rectangular waveguide, shown in Fig. 1, is given by[3]

$$\mathbf{E} = E_0 \sin\left(\frac{\pi}{a}x\right)\mathbf{a}_y \tag{1}$$

and the power carried by this mode is

$$P = E_0^2\,\frac{ab}{4}\sqrt{\frac{\epsilon_0}{\mu_0}}\sqrt{1-\left(\frac{c}{2\,af}\right)^2}\,, \tag{2}$$

where E_0 is the amplitude of the E-field at the center of the waveguide, a and b are the cross-sectional dimensions of the rectangular waveguide (where a is the larger dimension, see the inset in Fig. 1), f is the frequency, ϵ_0 and μ_0 are the permittivity and permeability of free space, and c is the speed of light *in vacuo*.

If E_0 can be measured, then the power can be determined. We can leverage the recent studies in the development of an atom-based, SI-traceable, approach for measuring E-field strengths, in which significant progress has been made in the development of a novel Rydberg-atom spectroscopic approach for RF E-field strength measurements.[4–13] This approach utilizes the phenomena of electromagnetically induced transparency (EIT) and Autler-Townes (AT) splitting,[4–6,14] and can lead to a direct SI traceable, self-calibrated measurement.

There are various ways of explaining the concept of this E-field measurement approach (see Refs. 5, 6, and 15 from an atomic physics viewpoint and Ref. 4 from a measurement viewpoint). Here, we only give a brief explanation, see those references for more details. Consider a sample of stationary four-level atoms illuminated by a single weak ("probe") light field, as depicted in Fig. 2. In this approach, one laser is used to probe the response of the atoms and a second laser is used to couple to a Rydberg state (the "coupling" laser). In the presence of the coupling laser, the atoms become transparent to the probe laser transmission (this is the concept of EIT). The coupling laser wavelength is chosen such that the atom is in a sufficiently high state (a Rydberg state) such that a radio frequency (RF) field coherently couples two Rydberg states (levels 3 and 4 in Fig. 2). The RF transition in this four-level atomic system causes a splitting of the transmission spectrum (the EIT signal) for a probe laser. This

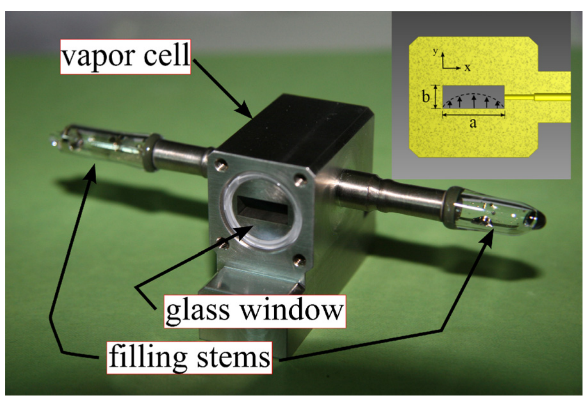

FIG. 1. WR-42 rectangular waveguide vapor cell with waveguide dimensions. The vapor cell consist of a 34-mm section of waveguide with glass windows attached to each end (and filled with ^{133}Cs.).

[a)]Electronic mail: christopher.holloway@nist.gov

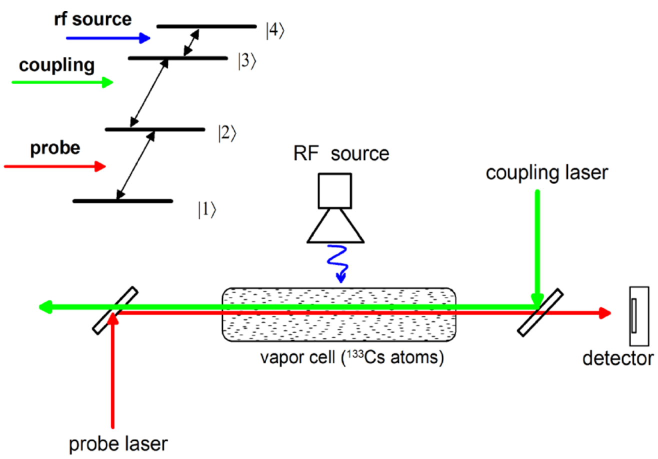

FIG. 2. Illustration of a four-level system and the vapor cell setup for measuring EIT, with the counter-propagating probe and coupling beams.

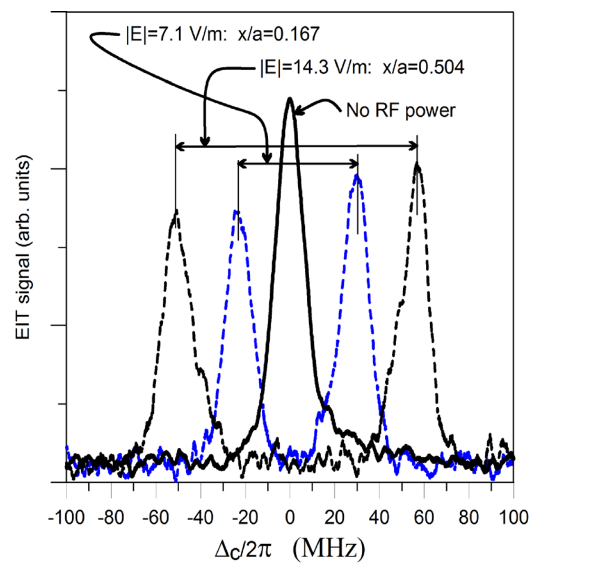

FIG. 3. Illustration of the EIT signal (i.e., probe laser transmission through the cell) as a function of coupling laser detuning Δ_c. This dataset is for 19.629 GHz and corresponds to this following 4-level atomic system: $6_{1/2} - 6P_{3/2} - 34D_{5/2} - 35P_{3/2}$. The dashed curves correspond to two different *x*-locations across the WR42 waveguide for an input power of −20.76 dBm.

splitting of the probe laser spectrum is easily measured and is directly proportional to the applied RF E-field amplitude (through Planck's constant and the dipole moment of the atom). By measuring this splitting (Δf_m), we get a direct measurement of the magnitude of the RF E-field strength for a time-harmonic field from Ref. 5

$$|E| = 2\pi \frac{\hbar}{\wp} \Delta f_m, \tag{3}$$

where $\hbar$ is Planck's constant, $\wp$ is the atomic dipole moment of the RF transition (see Refs. 5 and 17 for discussion on determining $\wp$ and values for various atomic states), and Δf_m is the measured splitting when the coupling laser is scanned. If the probe laser is scanned, a Doppler mismatch correction is needed in this expression.[14,15] We consider this type of measurement of the E-field strength a direct, SI-traceable, self-calibrated measurement in that it is related to Planck's constant (which will become a SI quantity defined by standard bodies in the near future) and only requires a frequency measurement (Δf_m, which can be measured very accurately and is calibrated to the hyperfine atomic structure).

A typical measured spectrum for an RF source with different E-field strengths is shown in Fig. 3. This figure shows the measured EIT signal for two E-field strengths (more details on these results are given below). In this figure, Δ_c is the detuning of the coupling laser (where $\Delta_c = \omega_c - \omega_o$; ω_o is the on-resonance angular frequency of the Rydberg state transition and ω_c is the angular frequency of the coupling laser). Notice that the AT splitting increases with increasing applied E-field strength. To obtain these results, we use cesium atoms (^{133}Cs) and the levels $|1\rangle$, $|2\rangle$, $|3\rangle$, and $|4\rangle$ correspond, respectively, to the ^{133}Cs $6S_{1/2}$ ground state, $6P_{3/2}$ excited state, and two Rydberg states. The probe is locked to the D2 transition (a 852 nm laser). The probe beam is focused to a full-width at half maximum (FWHM) of 290 μm, with a power of 3.2 μW. To produce an EIT signal, we apply a counter-propagating coupling laser (wavelength $\lambda_c \approx 510$ nm) with a power of 17.3 mW, focused to a FWHM of 380 μm. The coupling laser was scanned across the $6P_{3/2} - 34D_{5/2}$ Rydberg transition ($\lambda_c = 511.1480$ nm). We modulate the coupling laser amplitude with a 30 kHz square wave and detect any resulting modulation of the probe transmission with a lock-in amplifier. This removes the Doppler background and isolates the EIT signal, as shown in the solid curve of Fig. 3. Application of RF (details below) at 19.629 GHz to couple states $34D_{5/2}$ and $35P_{3/2}$ splits the EIT peak as shown in the dashed curves in the figure. The asymmetry in the EIT signal amplitude in the presence of the RF field is most likely due to Stark shifts. These small amounts of asymmetries do not affect the ability to use Eq. (3) to obtain accurate E-field strengths for low to moderate values; this is discussed in more detail below. These asymmetries can also arise for RF detuning, however, methods discussed in Refs. 16 and 17 were used to insure the RF signal is on resonance for the Rydberg states $|3\rangle$ and $|4\rangle$. We measure the frequency splitting of the EIT peaks in the probe spectrum Δf_m and determine the E-field amplitude using (3) as shown in Fig. 3. For this measurement, the dipole moment for the resonant RF transition is $\wp = 723.393 e a_0$ (which includes a radial part of $1476.619 e a_0$ and an angular part of 0.48989, which correspond to co-linear polarized optical and RF fields, where e is the elementary charge, $a_0 = 0.529177 \times 10^{-10}$ m, and is the Bohr radius).

Calculating $\wp$ requires one to first numerically solve the Schrödinger equation for the atomic wavefunctions and then a numerical evaluation of the radial overlap integrals involving the wavefunctions for a set of atomic states.[5,18] For a given atomic state, these numerical calculations require one to use the quantum defects (along with the Rydberg formula[18]) for the alkali atom of interest. Using the best available quantum defects[19–21] to perform a numerical calculation of $\wp$, it is believed that $\wp$ can be determined to less than 0.1%, which has been verified experimentally.[17]

In order to measure the power propagating down a WR42 rectangular waveguide, we placed a ^{133}Cs vapor cell in the waveguide system shown in Fig. 4. The experimental setup includes two 10 dB directional couplers, two RF tuners,

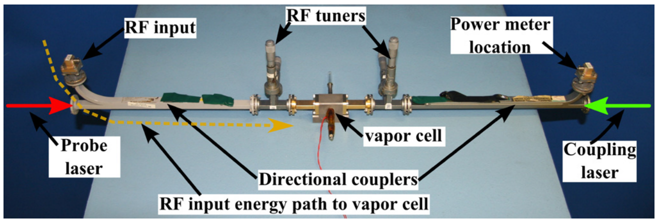

FIG. 4. Photos of the experimental setup for the vapor-cell filled waveguide.

and a 34 mm section of waveguide that serves as the vapor cell. The vapor cell consists of a 34-mm length of WR42 stainless-steel waveguide with glass windows attached to each end (attached with vacuum epoxy), see Figs. 1 and 4. The glass windows allow the vapor-cell waveguide to be filled with ^{133}Cs under vacuum. The directional couplers were used to allow the probe and coupling laser to propagate down the waveguide system and interact with the ^{133}Cs vapor, while at the same time allowing RF power to be coupled into the waveguide system (the directional coupler on the left) and allowing RF power to be coupled out of the waveguide system (the directional coupler on the right). The output of this second directional coupler was attached to a conventional RF power meter. The presence of the two windows on the vapor cell results in the possibility of RF standing waves (SWs) inside the vapor-cell along the propagation direction (along the waveguide axis). The RF tuners are used to minimize and eliminate these standing waves (discussed below). The RF energy path is as follows: the output of a RF signal generator is connected to the directional coupler on the left of Fig. 4 (labeled as the RF input). After propagating through this directional coupler and the first RF tuner, it passes through the vapor cell (34-mm sectional of waveguide containing ^{133}Cs) where it is measured using the EIT/AT approach. RF energy then propagates through the second RF tuner and into the last directional coupler. The curved section of this last directional coupler picks off about -10 dB (-10.44 dB at 19.629 GHz, and -9.88 dB at 26.562 GHz) of the input power and is then terminated into a power meter, see Fig. 4. The remaining power, that is not coupled into the power meter, propagates down the straight section of the directional coupler and radiates out of the end of the directional coupler. The RF absorber is placed 30 cm in front of the open-ended directional coupler (the absorber is used to absorb the radiated power in order to ensure that this radiated power is not reflected back into the coupler). Note that the coupler is left open in order to allow both the probe and coupling lasers to enter the waveguide setup and interact with the vapor cell section of the waveguide. While most of the power is radiated out of the coupler, there is some small faction of power reflected at the open-ended coupler, and this reflected power propagates back through the tuner and toward the vapor cell. As discussed below, the tuners are used to minimize any standing waves caused by these possible reflections.

The WR42 waveguide system has dimensions of $a = 10.668$ mm and $b = 4.318$ mm which allows for only one propagating mode (the fundamental TE_{10} mode) between 18 GHz and 27 GHz. Thus, we perform experiments for two frequencies in this range, i.e., 19.629 GHz and 26.526 GHz. We first perform experiments at 19.629 GHz which correspond to the $6S_{1/2} - 6P_{3/2} - 34D_{5/2} - 35P_{3/2}$ atomic system. The waveguiding system was placed on a translation-stage, which allowed the probe and coupling lasers to be scanned (while maintaining their counter-propagation alignment) across the x-axis of the waveguide. The EIT signal at two different x-axis locations in the waveguide is shown in Fig. 3. These results are for an input power (input to the directional coupler on the left, see Fig. 4) of -20.76 dBm. As discussed above, the presence of the glass windows can result in possible standing waves inside the vapor-cell. In order to get an accurate measurement for the forward propagating power, these standing waves needed to be eliminated (or at least minimized as much as possible). We can use the linewidth of the EIT signal as a means of determining when the standing wave (SW) effect is minimized. The SWs can result in a broadening of the EIT linewidth, a direct result of the inhomogeneous E-field variation (due to the SWs) along the propagation direction.[12] An inhomogeneous E-field along the direction of the laser beam propagation can cause a broadening of the EIT linewidth. To minimize this effect, we varied the RF tuners on both sides of the vapor-cell waveguide until the EIT linewidth was minimized, which was an indication when the RF SWs in the vapor-cell were minimized. The effect of the SWs on the EIT linewidth is shown in Fig. 5, where we show three EIT signals. One of the EIT signals is for the case when the RF tuners are optimized and the other two EIT signals are for the case when the RF tuners are non-optimized. We see that the EIT linewidth for the non-optimized cases is larger than the optimized case. Furthermore, the EIT signal shown in Fig. 3 is for the optimized tuners and we see that for this optimized case, the EIT linewidth is approximately the same as the case with no RF power in the waveguide, indicating that the RF SWs in the waveguide are minimized.

We next measure the E-field distribution across the x-axis in the waveguide for different input RF power levels. This is done by scanning the laser across the x-axis of the

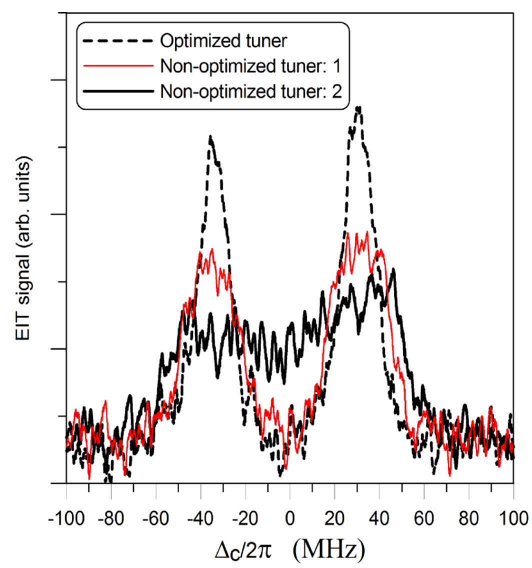

FIG. 5. The effects of the standing waves (inhomogeneous field) on the EIT line width. These results are for $x/a = 0.5$, 19.629 GHz, and an input power of -24.79 dBm.

waveguide from $x = 0$ to $x = a$ (actually scanning the waveguide system via the translation stage). The measured E-field distributions inside the waveguide for three different input powers (input to the directional coupler) are shown in Fig. 6. To obtain the results, we first measured Δf_m of the EIT signal at different x locations, then using Eq. (3), the E-field strength was determined. As indicated from Eq. (1), the E-field dependence should follow a $\sin(\pi x/a)$ distribution for the TE_{10} mode. The results in this figure indicate that the measured E-field distribution inside the waveguide follows this behavior very well.

With the E-field strength determined at the center of the waveguide (i.e., $x = a/2$), Eq. (2) can be used to determine the power flowing down the waveguide system. Figure 7 shows the measured RF power in the waveguide as a function of input power (i.e., the input power at the directional coupler on the left). These results are at 19.629 GHz and for a 4-level atomic system ($6S_{1/2} - 6P_{3/2} - 34D_{5/2} - 35P_{3/2}$) and with the same probe and coupling laser bandwidth and powers as that used above. As a comparison, we also show results obtained from a conventional power meter connected to the right directional coupler. The power-meter results were corrected for the losses in the waveguide system (i.e., loss and directional coupler attenuation). The comparison shows a very good agreement.

We performed a second set of measurements at 26.526 GHz. These experiments correspond to the following 4-level atomic system: $6S_{1/2} - 6P_{3/2} - 31D_{5/2} - 32P_{3/2}$. Once again the probe laser was locked to the D2 ^{133}Cs transient (a 852 nm laser) and the coupling laser was scanned across the $6P_{3/2} - 31D_{5/2}$ Rydberg transition ($\lambda_c = 511.787$ nm). The power and beamwidth for probe and coupling lasers were the same as used for 19.629 GHz. We first measured the E-field along the x-axis for the waveguide. While the results are not shown here, the results are similar to those for the 19.629 GHz case, i.e., following the expected $\sin(\pi x/a)$ behavior. With the E-field strength determined [using $\wp = 592.158 e a_0$ (which includes a radial part of $1208.737 e a_0$ and an angular part of 0.48989)] in the center of the waveguide (i.e., $x = a/2$), Eq. (2)

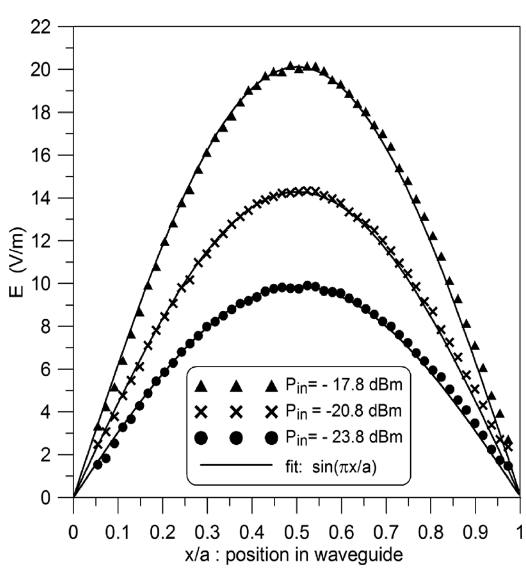

FIG. 6. E-field distribution along the x-axis of the waveguide at 19.629 GHz.

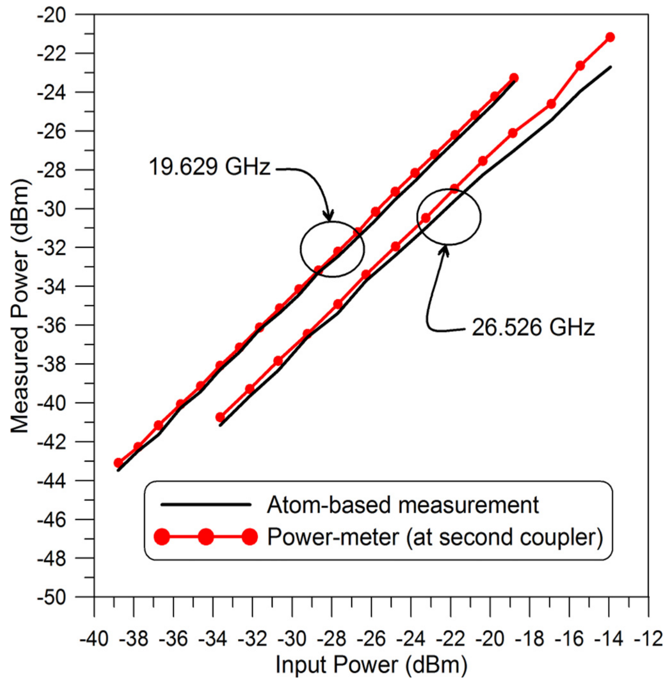

FIG. 7. Measurements power in the waveguide versus input power at both 19.629 GHz and 26.526 GHz.

can be used to determine the power flowing down the waveguide system. Figure 7 shows the measured RF power in the waveguide as a function of input power (i.e., the input power at the directional coupler on the left). Also, shown are the results from a conventional power-meter, where we see some discrepancies at the higher powers level for 26.526 GHz. Nevertheless, these results illustrate the ability to use Rydberg atoms to obtain the RF power inside a waveguide, which can lead to a SI-traceable method for determining RF power.

When the RF field levels become high (and stray electric and/or magnetic fields are present), one has to modify the approach for determining the E-field strength. Under these conditions, Eq. (3) is no longer valid and one needs to use a more elaborate model involving a Floquet analysis. In this approach, Stark maps from the Floquet model are fitted to measured Stark maps to determine the field strength. This type of a approach had been used in the past with great success for high E-field strength measurements and off-resonant fields.[12,13,22,23]

In the search for a quantum-based power standard, we have presented a fundamental different SI-traceable method for measuring RF power. The technique is based on Rydberg atomic vapor placed in rectangular waveguide and utilizing the EIT/AT approach. We first demonstrated the ability to measure the E-field distribution of the fundamental TE_{10} mode in the waveguide. We then performed measurements of RF power from the Rydberg-atom approach and compared it to results obtained from a conventional power meter. While perfect agreement is not shown for all the power levels tested and more work is needed to understand all the sources of error with this approach, the results here demonstrate the ability of this approach to measure RF power inside a waveguide, and can lead to a direct SI-traceable approach for power metrology. While the uncertainty of this measurement technique is currently being investigated, when compared to conventional power metrology approaches, this approach: (1) is a more direct SI traceable approach, (2) has the possibility of having much lower uncertainty, (3) exhibits much better frequency range, and (4) has much better dynamic range (i.e., power-level ranges). For high E-field values (i.e., high RF power), Stark shifts may become important and these effects may need to be incorporated into the method (a Floquet method) for the measurement of the fields and the determination the RF power.[12,13,22,23] The results in this paper are the first step towards the realization of a quantum-based RF power measurement technique and in the realization of a more direct link to the newly redefined SI.

[1]M. Stock, Meas. Tech. **60**(12), 1169–1177 (2018).
[2]See https://www.nist.gov/si-redefinition/road-revised-si for "Road To The Revised SI."
[3]C. T. A. Johnk, *Engineering Electromagnetic Fields and Waves* (John Wiley & Sons, NY, 1975).
[4]C. L. Holloway, M. T. Simons, J. A. Gordon, P. F. Wilson, C. M. Cooke, D. A. Anderson, and G. Raithel, IEEE Trans. Electromagn. Compat. **59**(2), 717–728 (2017).
[5]C. L. Holloway, J. A. Gordon, A. Schwarzkopf, D. A. Anderson, S. A. Miller, N. Thaicharoen, and G. Raithel, IEEE Trans. Antenna Propag. **62**(12), 6169–6182 (2014).
[6]J. A. Sedlacek, A. Schwettmann, H. Kübler, R. Löw, T. Pfau, and J. P. Shaffer, Nat. Phys. **8**, 819 (2012).
[7]C. L. Holloway, J. A. Gordon, A. Schwarzkopf, D. A. Anderson, S. A. Miller, N. Thaicharoen, and G. Raithel, Appl. Phys. Lett. **104**, 244102-1-5 (2014).
[8]J. A. Sedlacek, A. Schwettmann, H. Kübler, and J. P. Shaffer, Phys. Rev. Lett. **111**, 063001 (2013).
[9]H. Fan, S. Kumar, J. Sedlacek, H. Kübler, S. Karimkashi, and J. P. Shaffer, J. Phys. B: At. Mol. Opt. Phys. **48**, 202001 (2015).
[10]M. Tanasittikosol, J. D. Pritchard, D. Maxwell, A. Gauguet, K. J. Weatherill, R. M. Potvliege, and C. S. Adams, J. Phys. B **44**, 184020 (2011).
[11]C. G. Wade, N. Sibalic, N. R. de Melo, J. M. Kondo, C. S. Adams, and K. J. Weatherill, Nat. Photonics **11**, 40–43 (2017).
[12]D. A. Anderson, S. A. Miller, G. Raithel, J. A. Gordon, M. L. Butler, and C. L. Holloway, Phys. Rev. Appl. **5**, 034003 (2016).
[13]D. A. Anderson, S. A. Miller, A. Schwarzkopf, C. L. Holloway, J. A. Gordon, N. Thaicharoen, and G. Raithelet, Phys. Rev. A **90**, 043419 (2014).
[14]A. K. Mohapatra, T. R. Jackson, and C. S. Adams, Phys. Rev. Lett. **98**, 113003 (2007).
[15]C. L. Holloway, M. T. Simons, J. A. Gordon, A. Dienstfrey, D. A. Anderson, and G. Raithel, J. Appl. Phys. **121**, 233106-1-9 (2017).
[16]M. T. Simons, J. A. Gordon, and C. L. Holloway, Appl. Phys. Lett. **108**, 174101 (2016).
[17]M. T. Simons, J. A. Gordon, and C. L. Holloway, J. Appl. Phys. **120**, 123103 (2016).
[18]T. F. Gallagher, *Rydberg Atoms* (Cambridge University Press, Cambridge, 1994).
[19]P. Goy, J. M. Raimond, G. Vitrant, and S. Haroche, Phys. Rev. A **26**(5), 2733 (1982).
[20]K.-H. Weber and C. J. Sansonetti, Phys. Rev. A **35**, 4650 (1987).
[21]J. Deiglmayr, H. Herburger, H. Saßmannshausen, P. Jansen, H. Schmutz, and F. Merkt, Phys. Rev. A **93**, 013424 (2016).
[22]D. A. Anderson and G. Raithel, Appl. Phys. Lett. **111**, 053504 (2017).
[23]M. T. Simons, M. D. Kautz, C. L. Holloway, D. A. Anderson, and G. Raithel, J. Appl. Phys. **123**, 203105 (2018).